Applied Physics Letters

Strong coupling between Tamm plasmon polariton and two dimensional semiconductor excitons

Cite as: Appl. Phys. Lett. **110**, 051101 (2017); https://doi.org/10.1063/1.4974901
Submitted: 26 August 2016 • Accepted: 14 December 2016 • Published Online: 30 January 2017

Tao Hu, Yafeng Wang, Lin Wu, et al.

Strong coupling between Tamm plasmon polariton and two dimensional semiconductor excitons

Tao Hu, Yafeng Wang, Lin Wu, Long Zhang, Yuwei Shan, Jian Lu, Jun Wang, Song Luo, Zhe Zhang, Liming Liao, Shiwei Wu, Xuechu Shen, and Zhanghai Chen[a)]
State Key Laboratory of Surface Physics, Key Laboratory of Micro and Nano Photonic Structures (Ministry of Education), Department of Physics, Collaborative Innovation Center of Advanced Microstructures, Fudan University, Shanghai 200433, People's Republic of China

(Received 26 August 2016; accepted 14 December 2016; published online 30 January 2017)

Two dimensional (2D) semiconductor materials of transition-metal dichalcogenides (TMDCs) manifest many peculiar physical phenomena in the light-matter interaction. Due to their ultrathin property, strong interaction with light and the robust excitons at room temperature, they provide a perfect platform for studying the physics of strong coupling in low dimension and at room temperature. Here we report the strong coupling between 2D semiconductor excitons and Tamm plasmon polaritons (TPPs). We observe a Rabi splitting of about 54 meV at room temperature by measuring the angle resolved differential reflectivity spectra and simulate the theoretical results by using the transfer matrix method. Our results will promote the realization of the TPP based ultrathin polariton devices at room temperature. *Published by AIP Publishing.* [http://dx.doi.org/10.1063/1.4974901]

Strong coupling between photons and excitons, so called "exciton polariton," is a fascinating topic in solid state physics and has attracted much attention in recent years. Numerous novel phenomena have been observed, e.g., Bose Einstein Condensation of exciton polariton,[1–3] superfluidity,[4] quantum vortices,[5] entangled photon pairs,[6] polariton bistability,[7,8] etc. These exciting researches have also promoted the development of novel devices such as electrically injected polariton light emitting diode,[9–11] low threshold polariton laser,[12,13] spin-optronic devices,[14] optical switching,[15] polaritonic logic circuits,[16] etc.

In order to obtain well confined photons and thus observe the exciton-polariton effect, various optical microcavities, such as distributed Bragg reflector (DBR) based planar microcavity,[17] tunable open cavity,[18] two dimensional photonic crystal[19] and microdisk cavity with whispering gallery mode,[20] were designed. Recently, it is shown that one can also confine the light even without a cavity, e.g., a surface wave will form at the interface between a metal and a DBR. This is the so-called Tamm plasmon polaritons (TPPs).[21–24] In contrast to conventional surface plasmons, TPPs can be excited by direct optical excitation as their dispersion lies in the light cone given by $k = \omega/c$ where ω is the angular frequency, and k is the in-plane component of the wave vector of light, and TPPs have both TE and TM polarization. Moreover, since in the strong light-matter coupling regime Rabi splitting is proportional to the amplitude of the vacuum field, one can increase it through decreasing the mode volume. Compared with the traditional DBR-DBR cavity, the TPP mode gives a smaller mode volume[23] due to its surface wave nature.

The exciton polariton effect has been studied in various semiconductor microcavity systems, including ZnO[25,26] and GaN[27] with a large exciton binding energy which can work at room temperature. Meanwhile, the organic semiconductors also exhibit great prospects due to their strong exciton binding energies, high oscillator strengths, and high quantum yields.[28,29] Very recently, a new candidate for polaritonics, i.e., transition-metal dichalcogenides (TMDCs), has attracted much attention[30–34] due to their distinct electronic, mechanical, thermal, and optical properties when they are thinned to monolayer.[35] These materials change from an indirect to a direct bandgap with the transition from bulk to monolayer and the coupled spin and valley physics in monolayer TMDCs materials leads to the valley Hall effect.[36] Meanwhile, their robust excitons at room temperature thanks to their large exciton binding energy (0.5–1.0 eV), and the excellent optical qualities make them of great potential in the physics of strong coupling between light and matter at room temperature. Furthermore, due to the surface wave nature of the TPP mode, it is highly advantageous for the strong coupling with the 2D semiconductor materials. However, the strong coupling between the TPP mode and the monolayer TMDCs materials is yet to be demonstrated.

In this paper, we demonstrate the strong coupling between TPPs and the A excitons in monolayer MoS_2 and observe a Rabi splitting of about 54 meV at room temperature by angle resolved reflectivity spectroscopy. Theoretical simulation by using the transfer matrix method[21,22,37] agrees well with the experimental results.

Figure 1(a) shows the sample structure schematically. 10 pairs of HfO_2/SiO_2 DBR on the quartz substrate are grown by electron beam evaporation. The monolayer MoS_2 is exfoliated mechanically from bulk and then transferred onto the DBR by using polydimethylsiloxane (PDMS).[38] To form the TPP state, the top layer of TiO_2 of 56 nm and the silver film of 50 nm are deposited in the following electron beam evaporation process. In order to obtain the maximum coupling between TPP modes and the monolayer MoS_2, we need to position the MoS_2 layer in the region where the strongest amplitude of electric field is presented as shown in

a)Author to whom correspondence should be addressed. Electronic mail: zhanghai@fudan.edu.cn

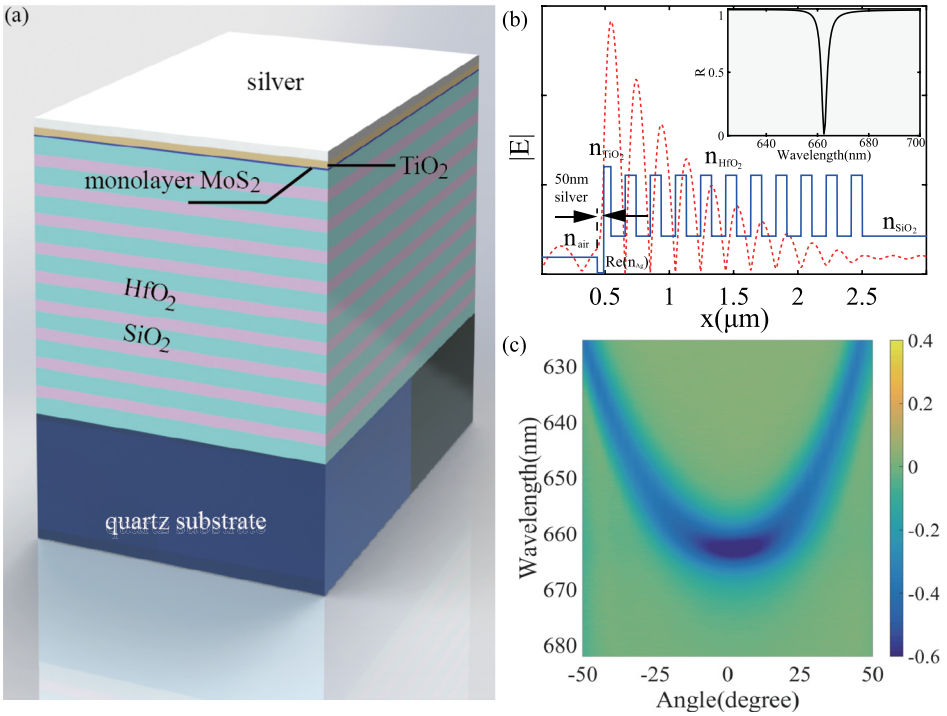

FIG. 1. (a) Schematic of the sample structure. (b) (Normal incidence) Theoretically calculated absolute electric field distribution of the TPP mode with a wavelength of 663 nm. The inset picture shows the reflectivity spectrum of the structure in (a) without monolayer MoS_2 embedded in it. (c) Experimentally detected angle resolved DRS of the TPP mode.

Figure 1(b). Via using the transfer matrix method, we give the theoretical calculation of the TE polarized TPP mode and the distribution of absolute electric field at normal incidence in Figure 1(b). The parameters used in the calculation are $n_{SiO_2} = 1.5$, $n_{HfO_2} = 1.95$, $n_{TiO_2} = 2.12$, and $n_{SiO_2} l_{SiO_2} = n_{HfO_2} l_{HfO_2} = \pi c/2\omega_0$, where ω_0 corresponds to the Bragg frequency with $\hbar\omega_0 = 1.87$ eV. The relative permittivity of silver is described by the Drude model

$$\varepsilon_{Ag}(\omega) = \varepsilon_\infty - \frac{\omega_p^2}{\omega^2 + i\gamma\omega}, \quad n_{Ag} = \sqrt{\varepsilon_{Ag}(\omega)}, \qquad (1)$$

where $\varepsilon_\infty = 5$, $\hbar\omega_p = 9$ eV, and $\hbar\gamma = 18$ meV. We confirm the TPP state in the structure by measuring the angle resolved differential reflectivity spectra (DRS) $\Delta R/R_0 = (R_{TPP} - R_0)/R_0$ (shown in Figure 1(c)), where R_{TPP} is the reflectivity of the TPP sample and R_0 is that of the silver reflector. The numerical aperture (NA) of the objective lens we use is 0.75 which allows us to detect the angular range of $\pm 48.6°$. The broadband light source is a tungsten halogen lamp and the angle resolved differential reflectivity spectroscopic setup is similar to that described in Ref. 32. From Figure 1(c), one can see a dip at 663 nm with half width at half maximum (HWHM) of $\hbar\Gamma_{TPP} = 14$ meV. This implies a quality factor of the TPP mode of 130 at a normal incidence. A parabolic dispersion of the TPP mode with the angle of the incidence light varying from 0° to 48.6° is observed.

The optical qualities of monolayer MoS_2 are examined by measuring the micro-photoluminescence (PL) spectroscopy and the DRS, as shown in Figures 2(a) and 2(b). In the PL experiments, the excitation is a 532 nm continuous wave laser line. From Figure 2(a), one can see two pronounced PL peaks at 652.5 nm and 610 nm associated with the A and B excitons, respectively,[39] and the dominant peak is 652.5 nm arising from the transition of the A excitons. The PL and Raman spectrum shown in Figure S1 (supplementary material) indicates the excellent optical quality of the monolayer MoS_2 and demonstrate that the thickness of exfoliated MoS_2 is a single layer.[40,41] In the measurement of the reflectance of our samples, the differential reflectivity is defined as $\Delta R/R_{sub} = (R_{sample} - R_{sub})/R_{sub}$, where R_{sample} is the reflectivity of the monolayer MoS_2 on the substrate (PDMS) and R_{sub} is that of the substrate. The two peaks in Figure 2(b) arise from the absorption of the A and B excitons which are consistent with the two peaks in Figure 2(a). Moreover, from the reflectance measurements of the samples, we can deduce the complex dielectric function of the monolayer MoS_2. The dielectric function of the monolayer MoS_2 is modelled by the multi-Lorentzian oscillators[42]

$$\varepsilon(\omega) = \varepsilon_b + \sum_{i=A,B} \frac{f_i}{\omega_i^2 - \omega^2 - i\Gamma_i\omega} = \varepsilon_1 + i\varepsilon_2, \qquad (2)$$

where ε_b is the background dielectric function, f is the oscillator strength, and the parameter i = A,B correspond to the A and B excitons in MoS_2. $\hbar\omega_A = 1.9$ eV, $\hbar\omega_B = 2.04$ eV, $\hbar\Gamma_A = 60$ meV, and $\hbar\Gamma_B = 110$ meV are fitted from the PL spectrum in Figure 2(a). By the simulation of the DRS (blue dashed line) which is in good agreement with the experimental result (orange dotted line), we can obtain the other parameters which are $\varepsilon_b = 18$, $\hbar^2 f_A = 1.7$ eV^2, $\hbar^2 f_B = 2.5$ eV^2. In the simulation, the refractive index of PDMS is set to be 1.5. The derived real and imaginary part of the complex dielectric function of the monolayer MoS_2 are given in Figure 2(c) which are consistent with the reported experimental results.[42]

By measuring the angle resolved DRS, we demonstrate the strong coupling between the TPP modes and A excitons in monolayer MoS_2. From Figure 3(a), two pronounced dips which correspond to the upper polariton branch (UPB) and the lower polariton branch (LPB) are seen at the angle of $\pm 38°$ when the TPP mode is resonant with the A excitons. The detailed part of the red rectangle in Figure 3(a) is

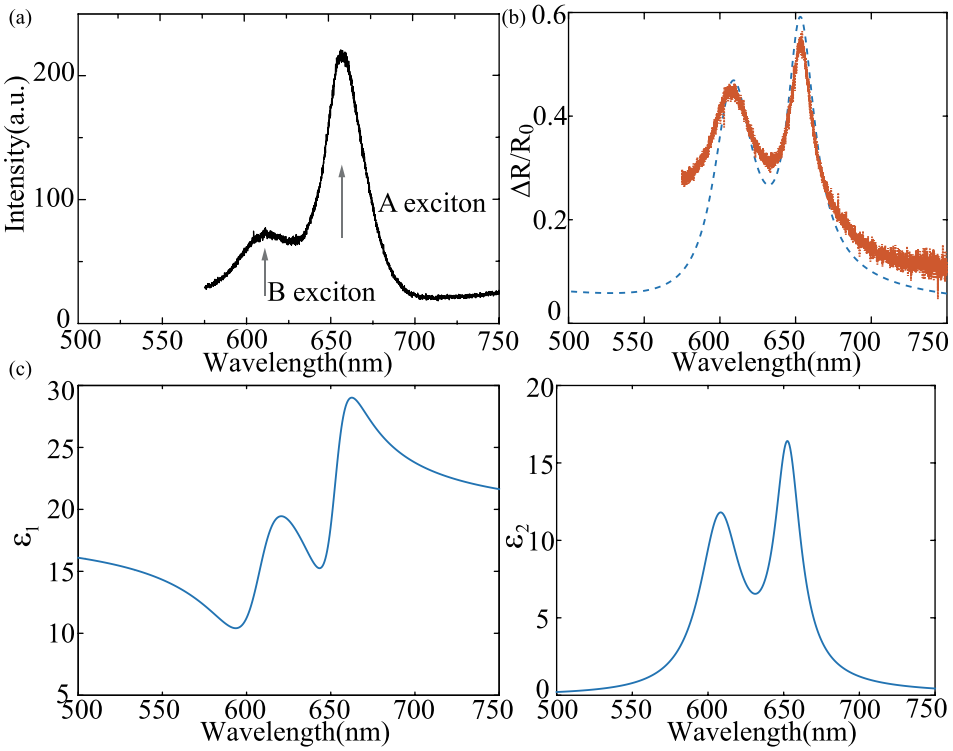

FIG. 2. (a) Photoluminescence of the monolayer MoS_2. The gray arrows indicate the A and B excitons in monolayer MoS_2. (b) The experimental (orange dotted line) and the theoretically simulated results (blue dashed line) of the the DRS of the monolayer MoS_2 on the PDMS substrate. (c) The real and imaginary parts of the complex dielectric function of the monolayer MoS_2.

displayed in Figure 3(b). With the increase of angle from 38° the UPB is more TPP like while the LPB is more exciton like and vice versa for the decrease of the angle from 38°. In Figure 3(a) only UPB is observed in large angle (>38°) and LPB in small angle (<38°), this is due to the broad linewidth of the A excitons at room temperature and the low contrast in the mapping of the DRS. For clarity, we extract the DRS of Figure 3(a) and fit the dips of these spectra. Three of the

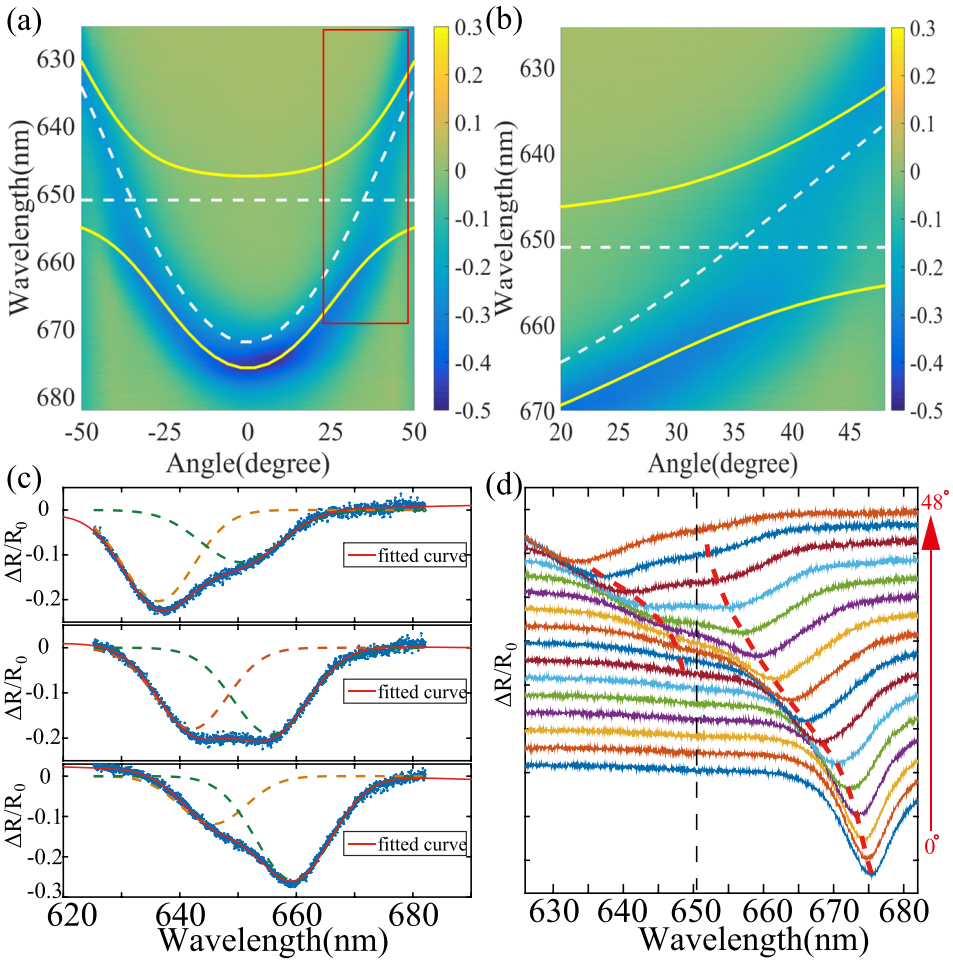

FIG. 3. (a) Angle resolved DRS of the TPP sample with the monolayer MoS_2 embedded in it. The white dashed line indicates the A exciton energy of MoS_2 and the dispersion of the TPP mode. The yellow lines represent the dispersion of the LPB and UPB. (b) The enlarged color map of the red rectangle in (a). (c) The fitted curves (red line) of the spectra extracted from (a) with an angle of 33°, 39°, and 45°, respectively. The orange dashed lines and green dashed lines are the Gaussian fitting of the UPB and the LPB, and the blue dotted lines are the experimental results. (d) Sixteen extracted spectra of (a) with an angle varying from 0° to 48°. The black dashed line shows the A exciton energy and the red dashed lines represent the fitted minima of each spectrum.

fitting results are shown in Figure 3(c) with an angle of 33°, 39°, and 45°, respectively, and two clear dips which are shown by the orange dashed line and green dashed line are seen in each spectrum. The fitting results from 0° to 48° are presented in Figure 3(d), and the red lines indicate the minima of these spectra. These dips reveal a clear anti-crossing feature when they approach the A exciton energy indicated by the black dashed line. We calculate the theoretical polariton dispersion with the coupling oscillator model expressed as[30]

$$\begin{pmatrix} E_{exciton} & V \\ V & E_{TPP}(\theta) \end{pmatrix} = E(\theta)\begin{pmatrix} a \\ b \end{pmatrix}, \tag{3}$$

where the $E_{exciton}$ is the energy of the A exciton, and $E_{TPP}(\theta)$ is the energy of the TPP mode which is calculated by using the transfer matrix method. V is the interaction strength between the TPP modes and A excitons in MoS_2. $E(\theta)$ is the eigen energy of the polariton branch given by

$$E_{LPB,UPB}(\theta) = \frac{1}{2}\left[E_{exciton} + E_{TPP}(\theta) \pm \sqrt{4V^2 + \left(E_{exciton} - E_{TPP}(\theta)\right)^2}\right] \tag{4}$$

and $|a|^2$, $|b|^2$ represents the exciton and TPP component of the corresponding polariton branch, respectively. The calculated dispersions are shown by the yellow lines in Figures 3(a) and 3(b). The white dashed line indicates the energy of the A excitons and the dispersion of the TPP mode. From the theoretical results, the detuning $\Delta E = E_{TPP} - E_{exciton} = -60$ meV and the fitted interaction potential V is about 27 meV indicating that the Rabi splitting $\hbar\Omega$ is 54 meV. To confirm the system is in the strong coupling regime, we extract the HWHM of the A excitons from the PL spectrum in Figure 2(a) with $\hbar\Gamma_A = 60$ meV. It is proved that the strong coupling condition for light-matter interaction is satisfied with $\hbar\Omega > (\hbar\Gamma_A + \hbar\Gamma_{TPP})/2$. However, the strong coupling between the TPP modes and the B excitons is not observed due to the large detuning between the TPP modes and B excitons.[30]

We also simulate the angle resolved DRS of the strong coupling between the A excitons and TPP modes by using the transfer matrix method which is given in Figure 4.

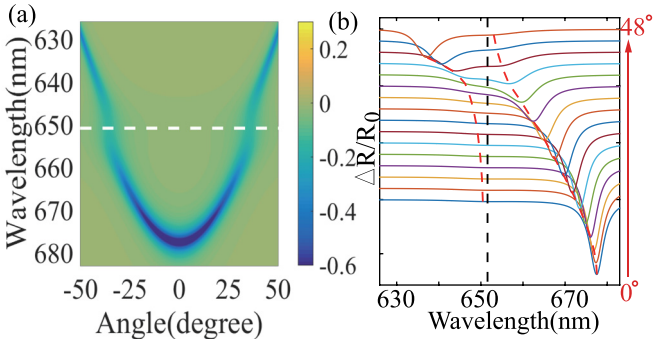

FIG. 4. (a) Simulated results of angle resolved DRS of the structure in Figure 1(a). The white dashed line indicates the A exciton energy of MoS_2. (b) Sixteen extracted spectra of (a) with an angle varying from 0° to 48°. The black dashed line shows the A exciton energy and the red dashed lines are the fitted minima of each spectrum.

During the simulation, the thickness of the monolayer MoS_2 is set to be 0.65 nm which is a common thickness for monolayer TMDC materials and the complex refractive index of monolayer MoS_2 is derived from Equation (2). The simulated results give features similar to the experimental results. The UPB is only observable at a large angle while the LPB is observable at a small angle from the color map in Figure 4(a). The extracted spectra in Figure 4(b) show a clear anti-crossing feature indicating the formation of the exciton polariton state. The vague in the spectra is mainly due to the broad linewidth of the A excitons at room temperature and the weak interaction strength between the TPP modes and the A excitons in the monolayer MoS_2 as the overlap between light field and the monolayer MoS_2 is very small due to the ultrathin property of 2D TMDCs materials. To confirm this, we increase the quality factor of the TPP mode with $\hbar\Gamma_{TPP} = 1.7$ meV and the calculated spectra in Figure S2(a) in the supplementary material are nearly the same as in Figure 4(a). That means the decreasing of the linewidth of the TPP modes from 14 meV to 1.7 meV does not increase the visibility of the LPB and UPB. Hence, we simulate the spectra with decreasing $\hbar\Gamma_A$ to 30 meV and 10 meV artificially which are shown in Figures S2(b) and S2(c) (supplementary material) with a clear LPB and UPB. If we enhance the oscillator strength such as utilizing the multi quantum well structure, the splitting between LPB and UPB can also be seen in the angle resolved DRS shown in Figure S2(d) (supplementary material). The simulation results of change of detuning are shown in Figure S3 (supplementary material).

The realization of strong coupling between photons and 2D semiconductor materials is of great importance due to the excellent optical qualities, stable excitons at room temperature, and the unique nature of the electron state of the 2D semiconductor materials. These materials provide a perfect platform for the investigation of exciton polariton effect in a low dimensional system and manipulation of exciton polariton emission by the valley degree of freedom. These unique properties will lead to the fabrication of novel controllable circular polarized polariton devices. Meanwhile, the electroluminescence of the 2D semiconductor has been reported in different structures[43–45] and the lasing actions[46–48] of such materials are also realized. Hence, the fabrication of the 2D semiconductor materials based polariton laser will be a challenging task in the future.

In summary, we demonstrate the strong coupling between the TPP mode and the A excitons in monolayer MoS_2 with a Rabi splitting of 54 meV. By measuring the angle resolved DRS, we observe the anti-crossing feature of the LPB and UPB indicating the formation of the exciton polariton state in the system. By using the transfer matrix method, we give the simulation of strong coupling effect which agrees well with the experimental results. The realization of strong coupling between TPP and 2D TMDC materials paves the way for the fabrication of real polariton devices in the TPP structure and reveal the possibility of electrically injected polariton laser in the future.

See supplementary material for more calculated strong coupling results between the TPP mode and the monolayer MoS_2.

The work is funded by the National Science Foundation for China (Nos. 11225419 and 91321311) and the Program of Shanghai Subject Chief Scientist (No. 14XD1400200).

[1]J. Kasprzak, M. Richard, S. Kundermann, A. Baas, P. Jeambrun, J. Keeling, F. Marchetti, M. Szymánska, R. Andre, and J. Staehli, Nature **443**, 409–414 (2006).
[2]R. Balili, V. Hartwell, D. Snoke, L. Pfeiffer, and K. West, Science **316**, 1007–1010 (2007).
[3]H. Deng, H. Haug, and Y. Yamamoto, Rev. Mod. Phys. **82**, 1489 (2010).
[4]A. Amo, J. Lefrère, S. Pigeon, C. Adrados, C. Ciuti, I. Carusotto, R. Houdré, E. Giacobino, and A. Bramati, Nat. Phys. **5**, 805–810 (2009).
[5]G. Nardin, G. Grosso, Y. Léger, B. Pietka, F. Morier-Genoud, and B. Deveaud-Plédran, Nat. Phys. **7**, 635–641 (2011).
[6]R. Johne, N. Gippius, G. Pavlovic, D. Solnyshkov, I. Shelykh, and G. Malpuech, Phys. Rev. Lett. **100**, 240404 (2008).
[7]D. Ballarini, M. De Giorgi, E. Cancellieri, R. Houdré, E. Giacobino, R. Cingolani, A. Bramati, G. Gigli, and D. Sanvitto, Nat. Commun. **4**, 1778 (2013).
[8]T. Espinosa-Ortega and T. C. H. Liew, Phys. Rev. B **87**, 195305 (2013).
[9]S. Tsintzos, N. Pelekanos, G. Konstantinidis, Z. Hatzopoulos, and P. Savvidis, Nature **453**, 372–375 (2008).
[10]L. Sapienza, A. Vasanelli, R. Colombelli, C. Ciuti, Y. Chassagneux, C. Manquest, U. Gennser, and C. Sirtori, Phys. Rev. Lett. **100**, 136806 (2008).
[11]C. Schneider, A. Rahimi-Iman, N. Y. Kim, J. Fischer, I. G. Savenko, M. Amthor, M. Lermer, A. Wolf, L. Worschech, V. D. Kulakovskii, I. A. Shelykh, M. Kamp, S. Reitzen, A. Forchel, Y. Yamamoto, and S. Hofling, Nature **497**, 348–352 (2013).
[12]P. Bhattacharya, B. Xiao, A. Das, S. Bhowmick, and J. Heo, Phys. Rev. Lett. **110**, 206403 (2013).
[13]P. Bhattacharya, T. Frost, S. Deshpande, M. Z. Baten, A. Hazari, and A. Das, Phys. Rev. Lett. **112**, 236802 (2014).
[14]I. Shelykh, G. Malpuech, K. Kavokin, A. Kavokin, and P. Bigenwald, Phys. Rev. B **70**, 115301 (2004).
[15]B. Piccione, C.-H. Cho, L. K. van Vugt, and R. Agarwal, Nat. Nanotechnol. **7**, 640–645 (2012).
[16]V. M. Menon, L. I. Deych, and A. A. Lisyansky, Nat. Photonics **4**, 345–346 (2010).
[17]R. Stanley, R. Houdre, U. Oesterle, M. Gailhanou, and M. Ilegems, Appl. Phys. Lett. **65**, 1883–1885 (1994).
[18]S. Schwarz, S. Dufferwiel, P. Walker, F. Withers, A. Trichet, M. Sich, F. Li, E. Chekhovich, D. Borisenko, and N. Kolesnikov, Nano Lett. **14**, 7003–7008 (2014).
[19]Y. Akahane, T. Asano, B.-S. Song, and S. Noda, Nature **425**, 944–947 (2003).
[20]K. Srinivasan and O. Painter, Nature **450**, 862–865 (2007).
[21]A. Kavokin, I. Shelykh, and G. Malpuech, Appl. Phys. Lett. **87**, 261105 (2005).
[22]M. Kaliteevski, I. Iorsh, S. Brand, R. Abram, J. Chamberlain, A. Kavokin, and I. Shelykh, Phys. Rev. B **76**, 165415 (2007).
[23]O. Gazzano, S. M. de Vasconcellos, K. Gauthron, C. Symonds, J. Bloch, P. Voisin, J. Bellessa, A. Lemaître, and P. Senellart, Phys. Rev. Lett. **107**, 247402 (2011).
[24]R. Brückner, M. Sudzius, S. Hintschich, H. Fröb, V. Lyssenko, M. Kaliteevski, I. Iorsh, R. Abram, A. Kavokin, and K. Leo, Appl. Phys. Lett. **100**, 062101 (2012).
[25]L. Sun, Z. Chen, Q. Ren, K. Yu, L. Bai, W. Zhou, H. Xiong, Z. Zhu, and X. Shen, Phys. Rev. Lett. **100**, 156403 (2008).
[26]W. Xie, H. Dong, S. Zhang, L. Sun, W. Zhou, Y. Ling, J. Lu, X. Shen, and Z. Chen, Phys. Rev. Lett. **108**, 166401 (2012).
[27]A. Das, J. Heo, M. Jankowski, W. Guo, L. Zhang, H. Deng, and P. Bhattacharya, Phys. Rev. Lett. **107**, 066405 (2011).
[28]S. Kéna-Cohen and S. Forrest, Nat. Photonics **4**, 371–375 (2010).
[29]P. Lagoudakis, Nat. Mater. **13**, 227–228 (2014).
[30]X. Liu, T. Galfsky, Z. Sun, F. Xia, E.-C. Lin, Y.-H. Lee, S. Kéna-Cohen, and V. M. Menon, Nat. Photonics **9**, 30–34 (2015).
[31]S. Dufferwiel, S. Schwarz, F. Withers, A. Trichet, F. Li, M. Sich, O. Del Pozo-Zamudio, C. Clark, A. Nalitov, and D. Solnyshkov, Nat. Commun. **6**, 8579 (2015).
[32]W. Liu, B. Lee, C. H. Naylor, H.-S. Ee, J. Park, A. C. Johnson, and R. Agarwal, Nano Lett. **16**(2), 1262–1269 (2016).
[33]N. Lundt, A. Maryński, E. Cherotchenko, A. Pant, X. Fan, S. Tongay, G. Sęk, A. Kavokin, S. Höfling, and C. Schneider, 2D Mater. **4**(1), 015006 (2016).
[34]X. Liu and V. M. Menon, IEEE J. Quantum Electron. **51**(10), 0600308 (2015).
[35]F. Xia, H. Wang, D. Xiao, M. Dubey, and A. Ramasubramaniam, Nat. Photonics **8**, 899–907 (2014).
[36]K. F. Mak, K. L. McGill, J. Park, and P. L. McEuen, Science **344**, 1489–1492 (2014).
[37]A. Kavokin and G. Malpuech, *Thin Films and Nanostructures* (Academic Press, 2003), Vol. 32.
[38]K. Choi, Y. T. Lee, S.-W. Min, H. S. Lee, T. Nam, H. Kim, and S. Im, J. Mater. Chem. C **1**, 7803–7807 (2013).
[39]K. F. Mak, C. Lee, J. Hone, J. Shan, and T. F. Heinz, Phys. Rev. Lett. **105**, 136805 (2010).
[40]A. Splendiani, L. Sun, Y. Zhang, T. Li, J. Kim, C.-Y. Chim, G. Galli, and F. Wang, Nano Lett. **10**(4), 1271–1275 (2010).
[41]Y. H. Lee, X. Q. Zhang, W. Zhang, M. T. Chang, C. T. Lin, K. D. Chang, Y. C. Yu, J. T. W. Wang, C. S. Chang, L. J. Li, and T. W. Lin, Adv. Mater. **24**(17), 2320–2325 (2012).
[42]Y. Li, A. Chernikov, X. Zhang, A. Rigosi, H. M. Hill, A. M. van der Zande, D. A. Chenet, E.-M. Shih, J. Hone, and T. F. Heinz, Phys. Rev. B **90**, 205422 (2014).
[43]Y. Ye, Z. Ye, M. Gharghi, X. Yin, H. Zhu, M. Zhao, and X. Zhang, *Science and Innovations* (Optical Society of America, 2014), Vol. STh4B, p. 4.
[44]J. S. Ross, P. Klement, A. M. Jones, N. J. Ghimire, J. Yan, D. Mandrus, T. Taniguchi, K. Watanabe, K. Kitamura, W. Yao, H. D. Cobden, and X. Xu, Nat. Nanotechnol. **9**, 268–272 (2014).
[45]R. Cheng, D. Li, H. Zhou, C. Wang, A. Yin, S. Jiang, Y. Liu, Y. Chen, Y. Huang, and X. Duan, Nano Lett. **14**, 5590–5597 (2014).
[46]O. Salehzadeh, M. Djavid, N. H. Tran, I. Shih, and Z. Mi, Nano Lett. **15**, 5302–5306 (2015).
[47]Y. Ye, Z. J. Wong, X. Lu, X. Ni, H. Zhu, X. Chen, Y. Wang, and X. Zhang, Nat. Photonics **9**, 733–737 (2015).
[48]S. Wu, S. Buckley, J. R. Schaibley, L. Feng, J. Yan, D. G. Mandrus, F. Hatami, W. Yao, J. Vúckovíc, A. Majumdar, and X. Xu, Nature **520**, 69–72 (2015).